Mean dynamic topography in the Southern Ocean: Evaluating Antarctic Circumpolar Current transport

A. Griesel,[1,2] M. R. Mazloff,[1] and S. T. Gille[1]

Received 8 September 2011; revised 23 November 2011; accepted 5 December 2011; published 28 January 2012.

[1] Mean Dynamic Ocean Topography (MDT) is the difference between the time-averaged sea surface height and the geoid. Combining sea level and geoid measurements, which are both attained primarily by satellite, is complicated by ocean variability and differences in resolved spatial scales. Accurate knowledge of the MDT is particularly difficult in the Southern Ocean as this region is characterized by high temporal variability, relatively short spatial scales, and a lack of in situ gravity observations. In this study, four recent Southern Ocean MDT products are evaluated along with an MDT diagnosed from a Southern Ocean state estimate. MDT products differ in some locations by more than the nominal error bars. Attempts to decrease this discrepancy by accounting for temporal differences in the time period each product represents were unsuccessful, likely due to issues regarding resolved spatial scales. The mean mass transport of the Antarctic Circumpolar Current (ACC) system can be determined by combining the MDT products with climatological ocean density fields. On average, MDT products predict higher ACC transports than inferred from observations. More importantly, the MDT products imply an unrealistic lack of mass conservation that cannot be explained by the a priori uncertainties. MDT estimates can possibly be improved by accounting for an ocean mass balance constraint.

Citation: Griesel, A., M. R. Mazloff, and S. T. Gille (2012), Mean dynamic topography in the Southern Ocean: Evaluating Antarctic Circumpolar Current transport, *J. Geophys. Res.*, *117*, C01020, doi:10.1029/2011JC007573.

1. Introduction

[2] Mean dynamic ocean topography (MDT) defines the mean stream function of the ocean's geostrophic surface flow. Since 1992, satellite altimeters have reliably provided measurements of the time-dependent variations in sea surface height, which represent the time-varying component of the dynamic ocean topography. However, altimeters are unable to detect the MDT, because most of the spatial variability in the time mean measured signal is associated with the Earth's geoid. Knowledge of the MDT is nonetheless critical for a number of reasons: in combination with altimetric sea surface height measurements the MDT provides the information needed to evaluate the absolute instantaneous streamlines, to assess eddy mean flow interactions, and to constrain dynamic sea surface height in ocean data assimilation. In this study we focus on the MDT in the Southern Ocean, which presents particular challenges due to a paucity of in situ observations, complex topography, strong variability, the presence of sea ice, and the prevailing strong winds that drive the Antarctic Circumpolar Current.

[3] In some altimetric studies, the MDT has been estimated from climatologies developed from in situ observations of the ocean's temperature and salinity fields [e.g., *Qiu*, 1995; *Sallée et al.*, 2008], but these fields have the disadvantage of depending on identifying a level of "no motion" or "known motion" [see, e.g., *Wunsch*, 1996] and may also be poor representations of mean conditions if in situ data are sparse or seasonally biased. Approaches based strictly on hydrographic data seem particularly likely to be problematic in the Southern Ocean, where historic data are sparse and where available in situ velocity observations suggest substantial nonzero bottom velocities [*Donohue et al.*, 2000; *Gille*, 2003; *Chereskin et al.*, 2009] that, to date, have not been well characterized.

[4] In the last decade, a variety of MDT products have been developed that rely on independent ocean velocity information and/or gravity data and therefore avoid depending on assumptions about flow at a reference level. These MDT products fall into three general categories, each of which presents its own difficulties. One category infers the MDT by combining surface drifter velocities with ship-based hydrographic data [*Niiler et al.*, 2003; *Rio and Hernandez*, 2003], but may be biased in regions with strong winds, either because the drogues experience a wind slip that is difficult to correct in the high-wind conditions of the Southern Ocean [e.g., *Niiler et al.*, 2003; *Elipot and Gille*, 2009] or because drogue losses have often remained undetected [*Grodsky et al.*, 2011]. A second category of MDT

[1]Scripps Institution of Oceanography, University of California, San Diego, California, USA.
[2]Also at Institute of Oceanography, University of Hamburg, Hamburg, Germany.

0148-0227/12/2011JC007573

Table 1. ACC Transport Estimates[a]

Reference	ACC Transport Estimate	Info
Georgi and Toole [1982]	137 Sv	SR1
Whitworth [1985]	134 ± 11.2 Sv	SR1
Cunningham et al. [2003]	136.7 ± 7.8 Sv	ISOS, SR1, deepest common level
Macdonald and Wunsch [1996]	142 ± 5 Sv	SR1, static inverse model
Ganachaud and Wunsch [2000]	140 ± 6 Sv	SR1, static inverse model
Sloyan and Rintoul [2001]	135 ± 1 Sv	SR1, static inverse model
Renault et al. [2011]	145 ± 8.8, 137.9 ± 10.5 Â Sv	SR1, direct velocity measurements
Ganachaud and Wunsch [2000]	157 ± 10 Sv	SR3, static inverse model
Rintoul and Sokolov [2001]	147 ± 10 Sv	SR3
Mazloff et al. [2010]	153 ± 5 Sv	SR1, assimilating model
Mazloff et al. [2010]	154 ± 5 Sv	SR2, assimilating model
Mazloff et al. [2010]	164 ± 6 Sv	SR3, assimilating model

[a]SR1, SR2, and SR3 are the identifiers for the World Ocean Circulation Experiment (WOCE) Southern Ocean repeat lines depicted in Figure 2.

product combines altimetry data with gravity data, the latter coming largely from the Gravity Recovery and Climate Experiments (GRACE) satellites with possible additional information from in situ gravity observations [e.g., *Tapley et al.*, 2003, 2005; *Pavlis et al.*, 2008], but no in situ oceanographic data. These MDT products have heightened uncertainty in regions of major ocean currents, as the scales associated with these flows are typically unresolved by GRACE. In situ gravity measurements can provide information about the geoid in these regions, but in the Southern Ocean few in situ gravity measurements have been made. A third category of MDT product represents a hybrid approach, which augments available altimetry and gravity observations with in situ oceanographic observations [e.g., *Rio and Hernandez*, 2004; *Maximenko and Niiler*, 2005; *Rio et al.*, 2009]. Since these products make use of a large range of relevant observations, they have the potential to produce an improved MDT, but the methods may not be sufficient to eliminate potential biases introduced by surface drifter wind slip. Moreover the sparseness of available in situ observations is problematic for suppressing eddy signals and determining the true MDT. For these hybrid approaches to be successful requires adequate knowledge of the error structure in each individual data set.

[5] In this study we evaluate the performance of four MDT products in the Southern Ocean, two based strictly on altimetry and gravity data and two hybrid products. Since MDT is nominally time invariant one might expect the four products to agree within formal uncertainty estimates. This is particularly true since all four products use GRACE satellite data and satellite altimetry data as a starting point, meaning that the bulk of the observations used to infer the MDT are similar in all products. Indeed, in parts of the Southern Ocean the four products show remarkable agreement. However, as this study shows, in other regions, we find substantial differences between the products, exceeding the order 10 cm uncertainty tested or estimated in recent studies [*Stammer et al.*, 2007; *Vossepoel*, 2007; *Andersen and Knudsen*, 2009].

[6] Independent observations are not available for the MDT, so there are no simple means to assess MDT products by comparing against "ground truth." One test is to consider whether MDT products are consistent with our knowledge of the large-scale ocean circulation. Ocean dynamics are largely in thermal wind balance. Thus, the ocean horizontal density gradient is proportional to the vertical shear of velocity: $\rho_y \propto u_z$. Although ocean velocity measurements are sparse, temperature and salinity (and thus density) observations have comparatively greater coverage, and this information can be used to determine geostrophic velocity relative to the velocity at a specified reference depth z_{ref}, as $u(z) = \int_{z_{ref}}^{z} (\partial_z u)dz + u(z_{ref})$. For this study, we use the MDT gradient to provide the geostrophic reference velocity at the ocean surface: $u(z_{ref}) = (g/f)\partial_y$MDT, where g is gravity and f is the Coriolis parameter. We then use hydrographic observations and the thermal wind relation to extend the ocean velocity estimates through the water column and determine total transport. Following oceanographic convention, we make the Boussinesq approximation of incompressibility, and thus volume conservation becomes the appropriate surrogate for mass conservation.

[7] ACC volume transport estimates typically range between 130 Sv and 150 Sv (see Table 1 or references of *Cunningham et al.* [2003] and *Mazloff et al.* [2010]). At a basic level, we expect the transport of the Antarctic Circumpolar Current to be consistent at all longitudes. Thus, the mean volume transport through Drake Passage (south of South America) should be approximately equal to the transport south of Africa, and should be about 10 to 20 Sv less than the transport south of Australia to account for the Indonesian Throughflow [e.g., *Georgi and Toole*, 1982; *Sprintall et al.*, 2009]. Our results will show otherwise: we find that the volume transport through these topographic constrictions is not conserved to within estimated uncertainty, thus implying that for this measure, the MDT products are inconsistent with ocean observations.

[8] A more refined approach to assessing MDT products is to ask whether they are consistent not just with ACC transport conservation constraints, but also more broadly with the full suite of dynamical and observational constraints employed in an assimilating ocean model. Assimilating ocean models determine best estimates of the ocean state that are consistent both with physics and observations. Best estimates of MDT that emerge from ocean data assimilation efforts have been used in a number of studies as benchmarks for evaluating MDT [*Bingham and Haines*, 2006; *Stammer et al.*, 2007; *Foerste et al.*, 2008; *Pavlis et al.*, 2008]. Here we make use of the Southern Ocean State Estimate (SOSE) [*Mazloff et al.*, 2010], which is a regional version of the MIT

Table 2. MDT Products, Mean Sea Surface and Geoid Product They Are Based on With Their Respective Time Periods, Resolution, Reference, and Type

MDT	MSS, Geoid Based on	Grid Resolution	Reference	Type in Short
EGM08	DNSC08B (1993–2004) GGM02C (Apr 2002 to Dec 2003)	1/60° × 1/60°	*Pavlis et al.* [2008]	geoid + altimetry
GGM02C	CLS01 (1993–2004) GGM02C (Apr 2002 to Dec 2003)	1/2° × 1/2°	*Tapley et al.* [2005]	geoid + altimetry
CNES-CLS09	MSS-CNES-CLS10 (1993–1999) EIGEN-GRGS.RL02 (Mar 2003 to Sep 2007) drifters (1993–2008) MDTs (1993–2007)	1/4° × 1/4°	*Rio et al.* [2009]	hybrid
MN05	drifters (1992–2002) GGM01 (Mar 2002 to Nov 2002)	1/2° × 1/2°	*Maximenko and Niiler* [2005]	hybrid
SOSE	2005–2007	1/6° × 1/6°	*Mazloff et al.* [2010]	assimilating

global circulation model (MITgcm; evolved from *Marshall et al.* [1997] that has been used extensively for global ocean state estimates [*Wunsch and Heimbach*, 2007]. We adopt a novel approach to constrain SOSE to all four MDT products simultaneously in order to cross compare their consistency in the optimization. The paper is organized as follows. Section 2 describes the MDT products that are analyzed and evaluates their differences. We discuss our attempt to bring them into consistency by accounting for the temporal sampling differences. In section 3 we combine the MDT products with hydrography to evaluate ACC transports and discuss uncertainties present in our transport calculation. The consistency of the SOSE and MDT products is assessed in section 4. We summarize our conclusions in section 5.

2. Comparison of Mean Dynamic Ocean Topography Products for the Southern Ocean

2.1. MDT Data Products

[9] We analyze four MDT products (Table 2) that are widely used in oceanographic research. All four make use of satellite gravity data collected by GRACE [e.g., *Tapley et al.*, 2003]. Here we introduce the products, discuss their temporal sampling, and assess root-mean-square differences between the products.

2.1.1. GGM02C

[10] GRACE consists of two satellites that orbit at 485 km above the surface, with a separation of 220 km. The satellites use a microwave ranging system to track small changes in their separation.

[11] GRACE data alone have been used to produce a gravity model identified as GGM02S [*Tapley et al.*, 2005]. We use an MDT product computed as the difference between the University of Texas Center for Space Research mean sea surface (CSRMSS98) and the GGM02C gravity field, which merges GGM02S with terrestrial gravity information (http://www.csr.utexas.edu/grace/gravity/ggm02/). This configuration produces a MDT field with a spatial resolution of about 500 km, and this resolution is limited by the elevation of the GRACE satellites, as well as measurement accuracy and satellite separation. Smoothing was needed in GGM02C to eliminate significant meridional striping [*Swenson and Wahr*, 2006]. For the Southern Ocean, where in situ gravity data are rare, GGM02S and GGM02C are expected to be effectively the same. Both the mean sea surface from altimeter observations and the geoid from GRACE are represented in spherical harmonics to degree and order 120 [*Tapley and Kim*, 2000], and the difference between them provides an estimate of the MDT. Although the spatial resolution is 300 km or less at degree and order 120, the MDT fields are smoothed, with a radius of influence of 500 km [*Tapley et al.*, 2005].

2.1.2. EGM08

[12] The Earth Gravitational Model 2008 (EGM2008), like GGM02C, is based on GRACE data, and also incorporates additional gravity and terrain data, which allows for higher spatial resolution in geographic regions where sufficient data are available. The MDT (here referred to as EGM08, while specified as DOT2008A on http://earth-info.nga.mil/GandG/wgs84/gravitymod/egm2008/oceano.html) is determined from the difference between the Danish National Space Center mean sea surface (DNSC08B) and the EGM2008 geoid [*Pavlis et al.*, 2008; *Andersen and Knudsen*, 2009]. While the use of supplemental data could in principle result in an MDT product with higher spatial resolution, in reality there have been virtually no in situ or airborne gravity measurements in the Southern Ocean, and EGM08 is not expected to have higher spatial resolution than GGM02C.

2.1.3. MN05

[13] One potential strategy for increasing the spatial resolution and reducing the uncertainty of the MDT is to use in situ oceanographic observations to refine the estimate derived from GRACE observations. *Maximenko and Niiler* [2005] derived an MDT estimate by combining the large-scale mean sea level based on GRACE and satellite altimetry with the mesoscale sea level tilt derived from the momentum balance as deduced from drifter, satellite altimeter, and wind data [*Maximenko and Niiler*, 2005; *Maximenko et al.*, 2009].

2.1.4. CNES-CLS09

[14] *Rio et al.* [2009] have developed an MDT product that is somewhat similar in concept to that of MN05. In their approach, a satellite-based MDT is first computed by subtracting the geoid model EIGEN-2 [*Reigber et al.*, 2003] from the mean sea surface height CLS01 (http://www.cls.fr/) determined from 7 years of altimetric data (TOPEX and ERS1,2) at spherical harmonic degree 30. This MDT is then refined to provide scales shorter than 660 km using oceanographic data. This solution serves as a first guess for the computation of a global and higher resolution MDT that combines in situ and altimetric data. The TOPEX/ERS1,2

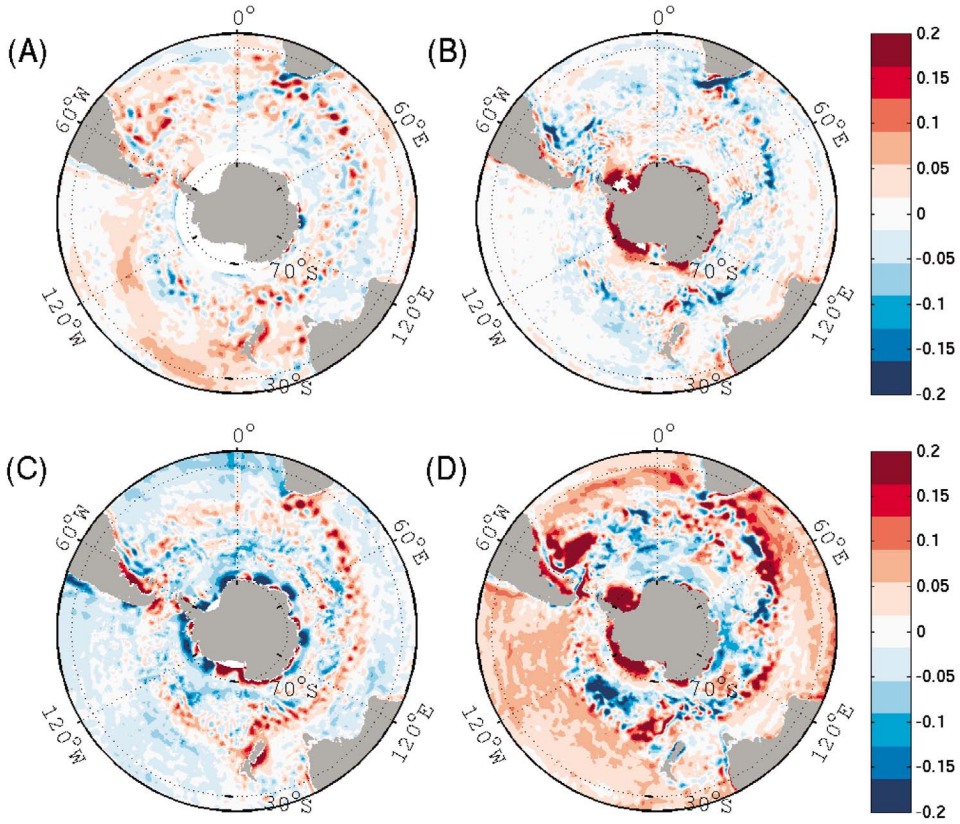

Figure 1. MDT differences from EGM08 in m. (a) EGM08-GGM02C, (b) EGM08-CNES-CLS09, (c) EGM08-MN05, and (d) EGM08-SOSE (prior to constraining SOSE to EGM08).

anomalies are subtracted from in situ measurements of the full dynamical signal (based on buoy velocities from the WOCE-TOGA and XBT, CTD). The resulting estimates of the local mean field are used to improve the first guess using an inverse technique [*Rio et al.*, 2009]. This MDT product is released by AVISO (http://www.aviso.oceanobs.com/).

2.1.5. SOSE

[15] Finally, we compare the four MDT products with the MDT that is determined by the Southern Ocean State Estimate (SOSE). SOSE is produced with the central purpose of attaining a best estimate of the Southern Ocean state for the years 2005 to 2007. The model is configured with 1/6° horizontal resolution, 42 vertical layers, and an open northern boundary. It is fit by constrained least squares to a large observational data set [*Mazloff et al.*, 2010]. The bulk of the constraints come from sea surface height anomaly and Argo observations, but also include derived sea surface temperature and sea ice concentration data as well as in situ profiles attained from CTDs, XBTs, and instruments mounted on elephant seals. Earlier iterations of SOSE did constrain to an MDT derived from the CLS01 mean sea surface and the EIGEN-GRACE03S geoid provided by M.H. Rio. This MDT is different from *Rio et al.* [2009] in that it does not include any ocean in situ observations. As explained in section 4, however, the a priori uncertainty prescribed to MDT constraints renders them rather noninfluential.

[16] An adjoint model is used to determine descent directions in minimizing a misfit function each of whose elements has been weighted by an estimate of the approximate observational plus model error [*Wunsch and Heimbach*, 2007]. The model is brought into near agreement with the data by adjusting its control vector, here consisting of initial and meteorological boundary conditions. In the SOSE solution model physics are a strong constraint that cannot be violated. Although total consistency has not yet been achieved, the existing 2005–2007 solution is in good agreement with the great majority of the observations, and thus it can be used to quantitatively estimate the properties of the Southern Ocean circulation [*Mazloff et al.*, 2010].

2.2. Scale Analysis and MDT Product Common Differences

[17] In order to carry out detailed comparisons, all MDT products are interpolated to the finer (1/6°) SOSE grid, and a constant offset equal to the average of each respective product between 64°S and 35°S is subtracted. The MDT differences reflect both large-scale differences in ACC strength and more localized differences along the path of the ACC (Figure 1). The standard deviation of the four products CNES-CLS09, MN05, EGM08 and GGM02C is ≤2 cm in 90% of the Southern Ocean. (Note that, since n is only 4, this standard deviation does not represent a statistically significant measure of the dispersion of MDT estimates.) However, it reaches ≥20 cm in localized areas where MDT gradients are high and the surface flow is restricted by topography, such as near the Kerguelen Plateau, south of New Zealand, and in the Agulhas Retroflection (Figure 2). Differences are also significant near the Antarctic coast which is likely an

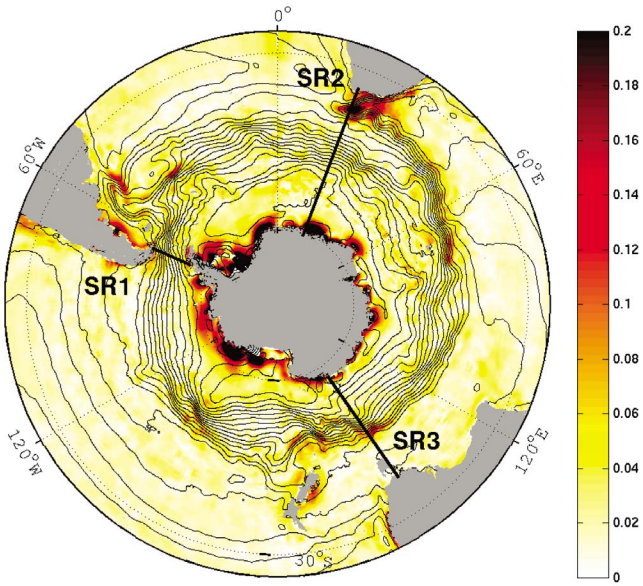

Figure 2. The mean (contours) and standard deviation (color) of the CNES-CLS09, MN05, EGM08, and GGM02C products (m). Also shown are horizontal sections corresponding approximately to WOCE SR1, SR2, and SR3.

artifact of the methods. (Altimetry can be unreliable near coasts and in the presence of sea ice.)

[18] The smallest root-mean-square (RMS) difference is between the two gravity-based products GGM02C and EGM08, as shown in Table 3. The two hybrid products CNES-CLS09 and MN05 show larger differences, and the greatest differences are between the four MDT products and the MDT diagnosed from SOSE (Table 3).

[19] Differences between MDT products may stem from their inclusion of observations from different time periods (Table 2). Geoid temporal variability is small, typically averaging less than 1 cm [*Chambers et al.*, 2004]. The temporal variability in the diagnosed mean sea surface, however, can be significant (order 10 cm) [*Andersen and Knudsen*, 2009]. To limit the differences in the MDT products arising from sea surface temporal variability, sea level anomalies, η, derived from satellite altimetry may be used to adjust the MDT products to represent a common time period T_c:

$$\mathrm{MDT}_{T_c} = \mathrm{MDT} + \left(\bar{\eta}_{T_C} - \bar{\eta}_{T_{\mathrm{MDT}}}\right), \qquad (1)$$

where the overline denotes temporal mean over the specific time period and the nominal time period of the MDT product is designated T_{MDT} (see Table 2). Here T_c is chosen to be 2005–2007, corresponding to the SOSE time period. In our calculations, we use gridded AVISO sea level anomalies (ASLA, http://www.aviso.oceanobs.com/) to compute $\left(\bar{\eta}_{T_C} - \bar{\eta}_{T_{\mathrm{MDT}}}\right)$.

[20] Counter to expectation, after applying the time corrections we find that the RMS differences between the MDT products increase rather than decrease (Table 3). As illustrated in the wave number spectra shown in Figure 3, the spatial scales of the MDT products (green, magenta, red, blue, black lines) and the ASLA MDT time correction fields

Table 3. RMS Differences of the Products[a]

Original Products					
EGM08	GGM02C	CNES-CLS09	MN05	SOSE	ORIG
0	2.85	3.95	5.08	8.89	EGM08
	0	4.61	5.19	8.86	GGM02C
		0	5.95	9.38	CNES-CLS09
			0	9.37	MN05
				0	SOSE
Time-Corrected Products					
EGM08	GGM02C	CNES-CLS09	MN05	SOSE	TCORR
0	2.85	4.04	5.08	9.17	EGM08
	0	4.80	5.20	9.15	GGM02C
		0	6.09	9.91	CNES-CLS09
			0	9.60	MN05
				0	SOSE

[a]In cm. In the time-corrected products, the correction was smoothed with a Gaussian with half radius of ≈460 km.

(cyan lines) differ. The five MDT products have a similar spectral structure for wavelengths longer than about 500 km. At shorter scales, the two gravity-only products (green and purple lines) are effectively smoothed and do not retain information below about 500 km, while SOSE (black line) and the hybrid products (red and dark blue lines) retain some energy at eddy scales. In contrast, the time correction fields (cyan lines) have low energy at high wavelengths, and at the shortest resolved scales, they show higher energy than all but the MN05 MDT product. (The energy in the short wavelengths in the MN05 MDT is likely noise resulting from merging high wave number in situ observations and low wave number gravity data. For most applications the short wavelengths in MN05 should be filtered.) In an attempt to better match scales we used a Gaussian filter (F),

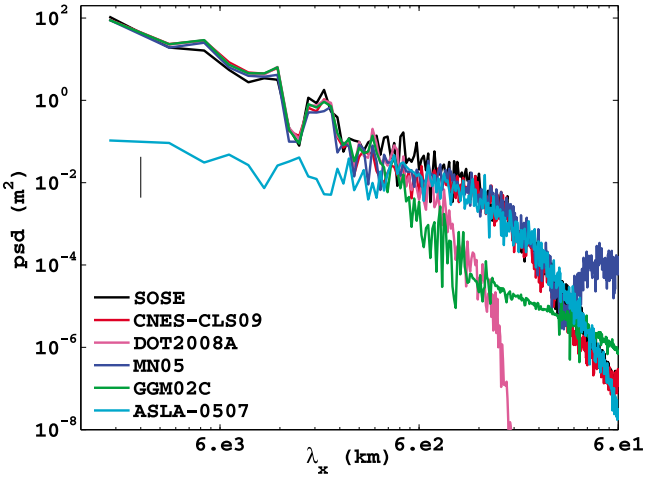

Figure 3. Zonal wave number power spectral density (PSD) estimates for the CNES-CLS09 (red), MN05 (blue), EGM08 (magenta), GGM02C (green) products and SOSE (black). Shown in cyan are the CNES-CLS09 sea level anomalies (ASLA). PSDs are computed by Fourier transforming 17 records from the circumpolar region without land points (~60°S–57°S) and then averaging the squared Fourier coefficients.

with a radius of decay $F(x) = 0.5$ at $x \approx 460$ km to smooth the ASLA. However, use of the smoothed time correction fields, MDT_{T_c}, still resulted in increased RMS differences between the products (Table 3). Since time corrections do not improve the compatibility of the products, we have not applied them in the analysis that follows. Determining how one should properly account for the temporal representation of the products, which likely requires accounting for more than just spatial resolution (e.g., accounting for temporal gaps due to sea ice) is left for future work. It is clear that the complexities that arise in accurately determining MDT [see, e.g., *Bingham et al.*, 2008] also arise in determining the time correction. For purposes where an MDT is needed to represent a specific time period, as opposed to a true long-term mean, it may be more practical for the user to subtract an altimetry-derived mean sea surface from a gridded geoid product. As explained in section 2.3, however, this too has drawbacks.

2.3. Uncertainty in Mean Dynamic Topography Products

[21] Formally, the squared MDT error is composed of the squared error of the mean sea surface σ^2_{ssh} and the squared error of the geoid, σ^2_{geoid}. In principle, there are commission errors that are in the resolved part of the data and omission errors that refer to the unresolved, unmodeled part. Geoid models are usually calculated as an expansion into spherical harmonic functions truncated at a certain degree, whereas sea surface height is a gridded product, additional complications arise when the two are combined, and some form of filtering must be applied [see, e.g., *Bingham et al.* 2008]. *Bingham et al.* [2008] compared two methods for combining mean sea surface and geoid, a pointwise approach where the gridded geoid is subtracted from the gridded mean sea surface, and a spectral approach where the spherical harmonics coefficients of the geoid are subtracted from an equivalent set of coefficients of the mean sea surface before gridding. They argue for the latter approach, since truncating the mean sea surface in the same way as the geoid ensures consistent truncation omission errors and retains more information, though it does introduce edge effects along the coasts that need to be removed.

[22] Satellite altimeter measurements of sea surface height depend on a number of independent observations, including the orbit, the so-called sea state bias (altimeter radar noise and electromagnetic and skewness biases), atmospheric corrections (i.e., ionospheric correction, wet and dry tropospheric corrections), and physical models of the ocean surface, as well as omission errors induced by the smoothing and aliasing of undersampled geophysical signals [e.g., *Ponte et al.* 2007]. *Chelton et al.* [2001] specified the total (mean and time variable) globally averaged error for each of these terms separately, with the largest being orbit error (2.5 cm), and the combined root-sum-of-squares error was estimated at 4.1 cm. Several of these terms are expected to vary considerably in space [e.g., *Tsaoussi and Koblinsky* 1994]. Furthermore, the separation of the altimeter error into time mean and residual is not unique, since temporally varying errors do not necessarily vanish with increasing averaging period: while the time-independent errors are typically below 2 cm, the risk of aliasing part of the time-varying signal into the mean is high, as the standard deviation of the time-varying component, the eddy error, is large, e.g., up to 25 cm in the Southern Ocean. The error budget of existing time mean dynamic topography estimates may now be dominated by residual errors in time mean altimetric corrections [*Stammer et al.*, 2007]. Understanding these errors requires intimate knowledge of how the mean sea surface was obtained, and there is much work to be done in producing accurate uncertainty estimates. For example, the formal error for the AVISO mean sea surface product MSS_CNES_CLS_10 is reported to be smaller than 2 cm over the Southern Ocean (http://www.aviso.oceanobs.com/), but our findings of differences of up to 20 cm between MDT products suggest that this formal error does not fully account for all aspects of the commission and omission errors.

[23] Uncertainties associated with the marine geoid have been reduced in recent years with the development of geoid models that represent an order of magnitude improvement in accuracy over previous satellite-based models [e.g., *Zhang and Lu*, 2005; *Pavlis et al.*, 2008]. By truncating the spectrum at some wave number, the total commission error is reduced at the cost of creating an error of omission, hence commission error increases with decreasing wavelength. The GRACE GGM01 commission error predicted at wavelength 360 km is 1 cm [*Zhang and Lu*, 2005].

[24] While geoid uncertainties have been characterized, MDT uncertainties are less readily available. The EGM08 RMS commission error over the global ocean was estimated to average 6.1 cm, with values smaller than 5 cm over most of the Southern Ocean, but 10–15 cm close to ice and land [*Pavlis et al.*, 2008]. Omission errors in the EGM08 product are not estimated, and, due to the Gibbs' phenomenon, may be significant even at long length scales [*Losch et al.*, 2002; *Bingham et al.*, 2008]. Neither of the hybrid products that we tested provides an uncertainty estimate, though *Maximenko et al.* [2009] compared a satellite based estimate of MDT and the hybrid estimates of *Rio and Hernandez* [2004] and *Maximenko and Niiler* [2005] and reported a global root-mean-square (RMS) difference of approximately 7 cm, with the largest difference south of 55°S. *Vossepoel* [2007] found global RMS differences between five observational MDTs to be between 4.2 to 10.5 cm, while reduction of differences between MDTs with increasing filtering scales was smaller than expected.

[25] Combining the above mentioned nominal (commission) errors for the mean surface and the geoid gives an upper bound of about 7 cm over most of the Southern Ocean away from land. The standard deviation between the products, which should be a lower bound as it omits errors common to all products, suggests, however, that this 7 cm upper bound of the nominal error is too small. Near complex topography and strong currents the standard deviation of the four products reaches 20 cm (Figure 2).

3. Assessing ACC Transports

[26] The ACC is by far the largest contributor to interoceanic exchange, and the three continents surrounding Antarctica each define a "choke point" of this exchange. The choke points, denoted in Figure 2 using the three WOCE Southern Repeat (SR) sections, are the Drake Passage between South America and the Antarctic Peninsula (SR1),

the SR2 line south of Africa, and the SR3 line south of Australia or New Zealand. Any differences in the volume transport through the choke points must be compensated by other interocean links. Because the interocean exchange provided by the flow through the Bering Strait is negligibly small [*Roach et al.*, 1995], flow through SR1 and SR2 is expected to be nearly identical, while the 10–20 Sv westward flow through the Indonesian Throughflow means that SR3 should carry a slightly larger transport [*Georgi and Toole*, 1982; *Sprintall et al.*, 2009].

[27] Geostrophic velocities in the ocean can be determined from the depth-dependent pressure gradient, which in turn can be integrated to determine transport. We separated the ACC transport into two components: a depth-independent contribution that depends only on the gradient of the surface height, η (i.e., the MDT), and a depth-dependent contribution that depends on the meridional in situ density gradients [see, e.g., *Griffies*, 2004]

$$\partial_y p(x,y,z) = g\partial_y(\rho_s \eta(x,y)) + g\int_z^0 \partial_y \rho(x,y,z')dz'. \quad (2)$$

This separation is common practice in ocean models as it separates the fast barotropic gravity waves that require smaller time steps from the much slower baroclinic fluctuations. Our equation (2) makes use of the reasonable assumption of a vertically well-mixed surface layer with constant density, ρ_s, such that $\int_0^\eta \rho(x,y,z')dz' = \rho_s\eta$. In the following, we further approximate the surface density to be spatially constant, ρ_0, so that contributions to the depth-independent transport from horizontal surface density gradients are assumed negligible. Then, the geostrophic zonal ACC transport is separated into a depth-dependent contribution, U_{bc}, that depends on the meridional density gradients and is depth dependent but independent of MDT, and a depth-independent contribution, U_{bt}, due to the surface height gradient. For readability, we refer to the depth-dependent component as baroclinic, and to the depth-independent component as barotropic, though this is not rigorously how these components are defined. The vertically integrated velocities are determined as follows:

$$U_{bc} = -g/(f\rho_0)\int_z^0 \partial_y \rho dz, \quad (3)$$

$$U_{bt} = -g/(f\rho_0)\partial_y(\rho_s\eta) = -(g/f)\partial_y\eta. \quad (4)$$

[28] Note that the baroclinic transport as defined here differs from some other studies' usage of the term, in which transports are calculated by integrating thermal wind up from the ocean floor [e.g., *Cunningham et al.*, 2003]. In some cases, Southern Ocean studies have assumed geostrophic transport to be negligible at the ocean floor [e.g., *Georgi and Toole*, 1982; *Cunningham et al.*, 2003].

[29] The total geostrophic ACC transport is thus given by

$$T_g = \int_{y_1}^{y_2}\int_{-H}^{0} (U_{bc} + U_{bt})dzdy. \quad (5)$$

We determine U_{bt} using the MDT products, and estimates of U_{bc} are obtained from SOSE density gradients or from the WOCE 98 [*Gouretski and Jancke*, 1998] (hereafter referred to as GJ98) climatology. Baroclinic transports from several CTD sections were also evaluated in attempt to gauge uncertainty.

3.1. Transport Differences

[30] Figure 4 shows MDT along constant longitudes close to the three WOCE Southern Repeat sections. Transport calculations are sensitive to the integration endpoints y_1 and y_2 in equation (5). In order to minimize the influence of southern endpoints, we calculated transports with respect to the zero contour of the SOSE vertically integrated geostrophic transport stream function (southern vertical lines in Figure 4 and southernmost contour in Figure 5). To assess uncertainty with respect to the endpoints, we also calculated transports for other y_1 and y_2 limits, as discussed in section 3.2.

[31] The transports through the Southern Ocean constriction points determined using the MDT products vary widely. Baroclinic transports calculated from GJ98 are consistently weaker than in SOSE, owing to consistently smaller shear in GJ98 (Figure 6). The transports using the SOSE baroclinic state are, in general, more consistent with previous magnitude inferences so we discuss these numbers, though both estimates are given in Table 4. Cumulative transports in Figure 7 show differences in frontal locations, resolution, and current strengths. The location and strength of the Agulhas Current system for example varies widely between products (Figures 7c and 7d). The transport estimates using the CNES-CLS09 and MN05 products are larger than that inferred using the SOSE MDT for SR1 and SR3, but lower for SR2. Using the GGM02C product the transport is larger than SOSE through SR2 and SR3, but lower for SR1. The differences are substantial, and as we discuss in section 3.2, are statistically significant.

[32] Furthermore, the transport calculation yields significant implied divergence between the sections. As noted in the introduction, the ACC system exhibits relatively little divergence [*Mazloff et al.*, 2010], meaning that the flow between SR1 and SR2 should be consistent within uncertainty. The flow between these sections and SR3 should also be consistent, with the caveat that SR3 should be larger by approximately 10–20 Sv due to the Indonesian Throughflow. The MDT products, however, imply large divergences and are inconsistent between constriction points. Using the SOSE baroclinic state, which gives a result more consistent with volume conservation than does GJ98, the CNES-CLS09 MDT implies a 37 Sv divergence between SR1 and SR2. EGM08 has a divergence of 15 Sv between this section, and a 31 Sv divergence between SR2 and SR3. GGM02C has a divergence of 46 Sv between SR1 and SR2. MN05 yields a divergence of 61 Sv between SR1 and SR2, and a 99 Sv divergence between SR2 and SR3. The divergences often increase even further when density gradients from the GJ98 climatology are used (Table 4).

[33] With the exception of the 10–20 Sv divergence in the Indo-Pacific region due to the Indonesian Throughflow, ACC divergence is not expected at any longitude. To illustrate the larger picture and try to determine where mass conservation is being broken, we plot the 140 Sv transport contour in Figure 5. There are regions where this contour is found at similar latitudes for all products. However, there are

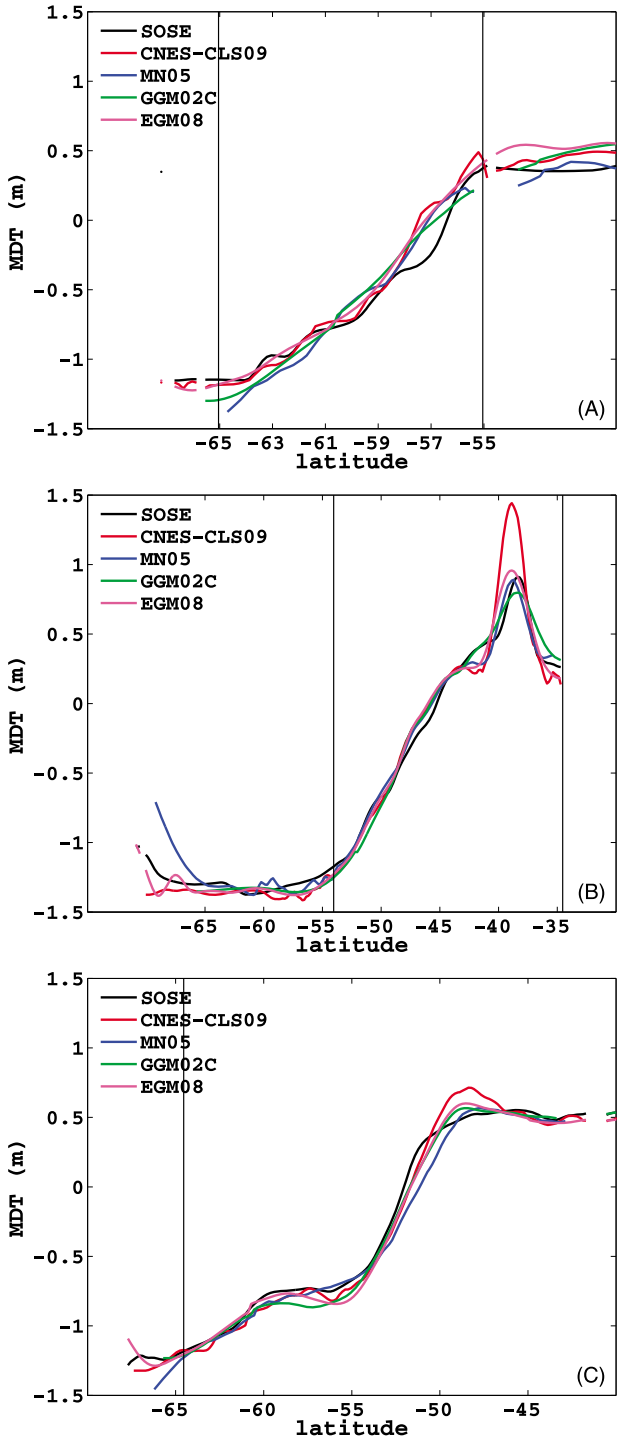

Figure 4. MDTs along (a) SR1, (b) SR2 and (c) SR3 (see Figure 2). SOSE (black), CNES-CLs09 (red), MN05 (blue), GGM02C (green), and EGM08 (magenta). The black vertical lines denote the limits used for ACC transport calculations.

other regions (e.g., the southeast Pacific), that are characterized by diverging contours. In these regions total transport estimates determined from the MDT products combined with hydrography are inconsistent with mass conservation. Figure 5 also shows that for most longitudes, the 140 Sv streamline is further north in the pure SOSE results than in results derived using any of the four MDT products to

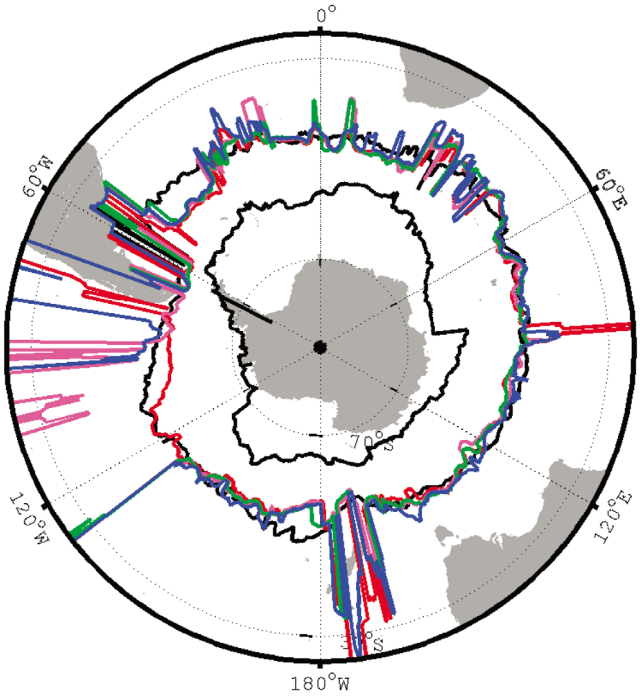

Figure 5. Latitudes of 140 Sv contours when transports are based on zero contour of SOSE geostrophic stream function (black southernmost contour), for EGM08 (magenta), GGM02C (green), CNES-CLS09 (red), MN05 (blue) and SOSE (black) (SOSE baroclinic transport used for all). Large jumps in the 140 Sv contour implies unphysical mass divergences in the derived transports.

determine U_{bt}. This implies that for most longitudes, all four products have larger meridional MDT gradients across the ACC.

3.2. Uncertainties in Transport Calculation

[34] Formally, from equations (3), (4), and (5), the uncertainty in geostrophic transport is composed of the

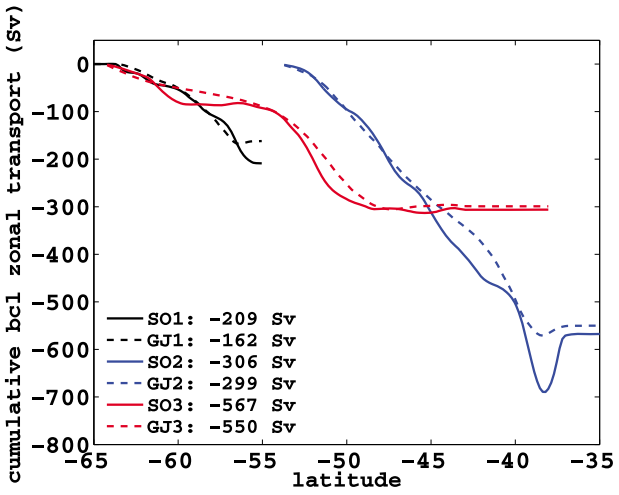

Figure 6. Zonal baroclinic ACC transports as defined in equation (3) for SOSE (solid lines) and GJ98 (dashed lines) and SR1 (black), SR2 (blue), and SR3 (red).

Table 4. Summary of ACC Transports Using SOSE Baroclinic Transports and GJ98 Using the Zero Contour of SOSE Geostrophic Streamline[a]

	SR1 Drake	SR2 Africa	SR3 Tasmania	SR1-SR2
CNES-CLS09	172 ± 6 (224)	135 ± 31 (169)	164 ± 4 (188)	37 (55)
EGM08	151 ± 3 (205)	136 ± 13 (166)	167 ± 4 (194)	15 (39)
GGM02C	142 ± 2 (182)	188 ± 23 (219)	175 ± 3 (200)	46 (37)
MN05	159 ± 4 (211)	98 ± 18 (133)	187 ± 7 (213)	61 (78)
SOSE	147 ± 5	145 ± 15	159 ± 3	2

[a]See Figure 5. The numbers in parentheses are for GJ98. The error given is the standard deviation of the transport 1° around southern and northern endpoints. Note that SOSE values differ from the ones given in Table 1, where transports were calculated from meridional and vertical integration of velocities directly (see text).

uncertainties in $\partial_y\eta$, $\partial_y\rho$, H, and dy. In a simplified way, the uncertainty in geostrophic transport may be summarized in three terms:

$$\sigma^2_{T_g} = \sigma^2_{T_{bt}} + \sigma^2_{T_{bc}} + \sigma^2_{T_{dc}}, \tag{6}$$

where $\sigma_{T_{bt}}$ is the uncertainty in the MDT, $\sigma_{T_{bc}}$ is the uncertainty in the density, and $\sigma_{T_{dc}}$ is the uncertainty associated with discretization (the gridding, ocean depth, and meridional distance). While errors in these three terms could be correlated, they each result from distinctly different processes, and it is a reasonable approximation to treat them as uncorrelated variables; if the terms were correlated, then the effect would be to slightly reduce the size of $\sigma^2_{T_g}$.

[35] In transport estimates, in addition to MDT commission and omission errors, uncertainties also arise from mapping procedures and subsequent area integration of the transport-related variables. Transport estimates are sensitive to the accuracy of discretized ocean depth and the integration endpoints y_1 and y_2 in equation (5).

[36] To estimate $\sigma_{T_{dc}}$, we can compare the transport calculated from the mean zonal velocity in SOSE directly, with the geostrophic transport calculated a posteriori from the SOSE mean temperature, salinity and sea surface height. As shown in Table 4, the zonal geostrophic SOSE ACC transport is 147 Sv for SR1 and 145 Sv for SR2. The ACC transport calculated from the total velocity is 150 Sv for the 2005–2007 mean for these sections. Ageostrophic components of the velocity account for no more than 1 Sv, and we attribute the rest of the difference of up to 4 Sv to discretization error from the a posteriori calculation of the geostrophic transport with a slightly different grid and land mask. The choice of endpoints y_1 and y_2 also matters for the transport estimate. From Table 4 the uncertainty is in the range of up to about 8 Sv when uncertainty in the endpoints is about 1° latitude. The exception is the northern endpoint of the SR2 section, where the net zero transport of the Agulhas leakage has to be properly accounted for. A liberal estimate for the discretization error seems to be $\sigma_{T_{dc}} \sim 10$ Sv.

[37] Once the variables are discretized, the uncertainty in the barotropic transport due to the uncertainty in the gradient of MDT needs to be taken into account. Thereby, the error close to land and ice of MDT is larger than for the interior ocean. An estimate of uncertainty can be made by considering that the barotropic transport $T_{bt} = \int_{y_1}^{y_2}\int_{-H}^{0}(-gf^{-1}\partial_y\eta)\,dzdy$, and by assuming a constant ocean depth H, $\sigma_{bt} \sim (-g/f)H\sigma_\eta$. Choosing H = 3000 m and σ_η to be 5 cm results in an estimate of $\sigma_{T_{bt}} \sim 20$ Sv.

[38] To estimate $\sigma_{T_{bc}}$ we can use the differences in GJ98 and SOSE baroclinic transports, T_{bc}. These differences are up to 40 Sv, because GJ98 has smaller baroclinicity than SOSE as a result of smoothing and low resolution. These differences, however, overestimate the uncertainty in the SOSE T_{bc} that we are using for our estimate. Another way to gauge the uncertainty of the mean T_{bc} comes from the standard deviation in time from the WOCE lines. At SR1, *Cunningham et al.* [2003] found the uncertainty of transports relative to the deepest common level to be ±7.8 Sv, based on the standard deviation of baroclinic geostrophic transports. Similarly at SR3, *Rintoul and Sokolov* [2001] calculated the baroclinic transport uncertainty to be ±10 Sv. On this basis, we estimate the baroclinic transport uncertainty $\sigma_{T_{bc}}$ to be ∼10 Sv.

[39] In total, we estimate the geostrophic transport uncertainty, σ_{T_g}, to be about 24 Sv, on the basis of the summed squares of the discretization error, nominal errors for the MDT, and the standard deviation in T_{bc}. The transport determined here using MDT products (Table 4) is on the high end of previous inferences (Table 1), though with $\sigma_{T_g} \sim$ 24 Sv they are for the most part consistent (possible exceptions being CNES for SR1 and MN05 for SR3). A primary concern is that the divergence implied by the MDT calculations substantially exceeds 24 Sv, and even the $24\sqrt{2}$ Sv = 34 Sv as would be the uncertainty for a difference of two independent observations. In reality, errors at the three choke points are expected to be correlated, and therefore we expect the divergence between lines to be less than 34 Sv. The divergence of ACC transport determined from the combination of MDT products with the SOSE baroclinic state exceeds this liberal uncertainty estimate, implying a failure of mass conservation.

4. Fit to SOSE

[40] One test of MDT products is to evaluate the extent to which ocean circulation in SOSE can be made consistent with them. SOSE has always imposed an MDT constraint; earlier iterations included a cost function term penalizing the weighted misfit squared between an observationally estimated MDT (CLS01 mean sea surface and the EIGEN-GRACE03S geoid had been used) and the computed SOSE MDT, $(\bar{\eta}_{\mathrm{SOSE}} - \bar{\eta}_{\mathrm{MDTproduct}})^2\sigma^{-2}$. For this study, we modified the MDT cost function to constrain SOSE to all four MDT products, assuming no time correction. We also implemented a fifth constraint, using the EGM08 MDT with the proper time correction. In our calculations, the uncertainty estimate, σ, was the standard deviation of the products (Figure 2), but capped not to go below 5 cm.

[41] Ten iterations of SOSE were completed using this modified constraint. Due to the magnitude of these uncertainty estimates (i.e., weighting in the least squares optimization) the MDT constraints were weak, accounting for only about 1.3% of the total constraints, while the bulk of the constraints resulted from in situ temperature and salinity observations and also sea level anomaly observations. The resulting costs (i.e., weighted mean squared misfits) associated with the MDT product are given in Table 5. Because the differences between the MDT products are smaller than the

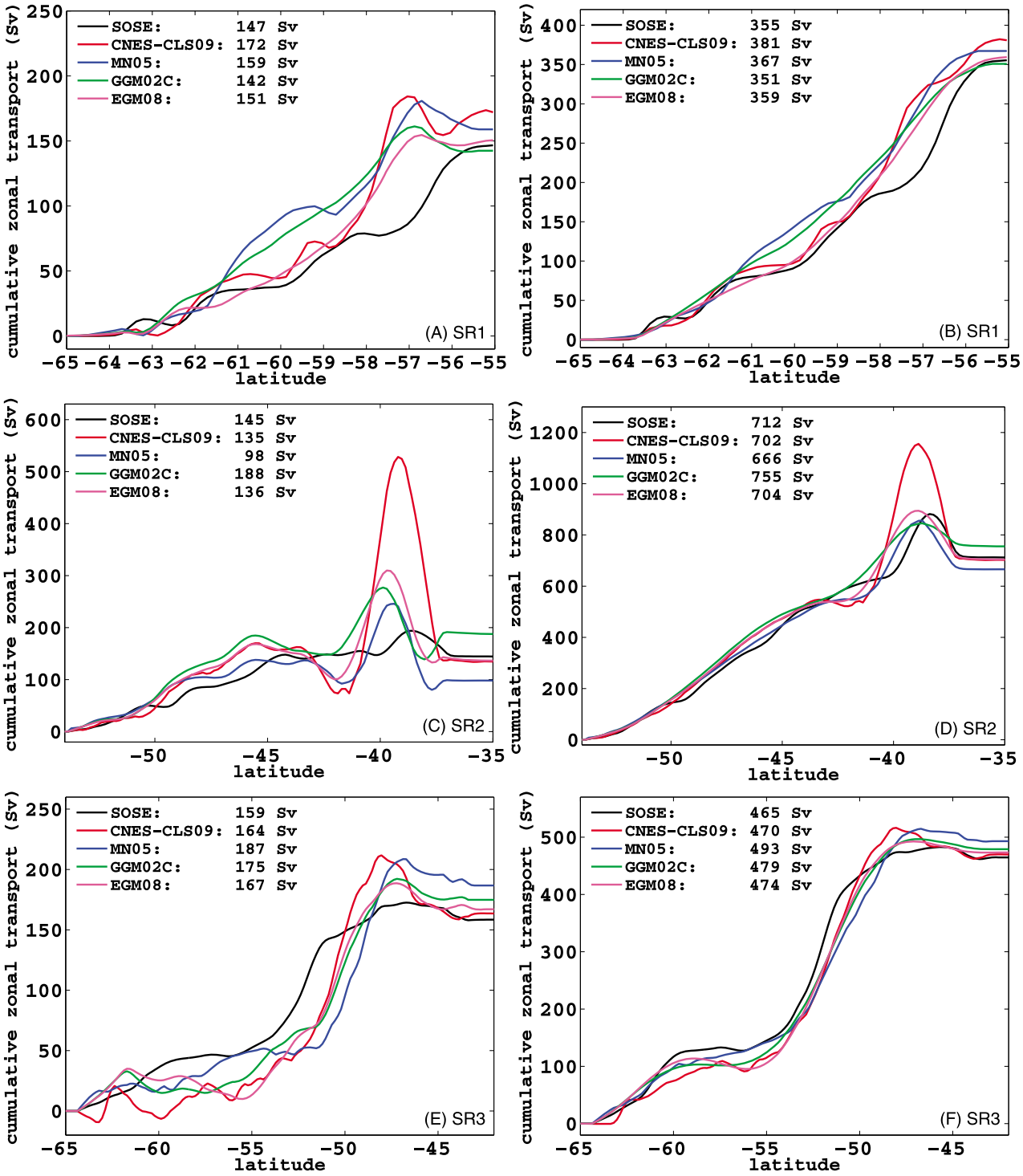

Figure 7. (left) Cumulative zonal ACC transports, calculated from MDT gradients and SOSE density gradients for the data products for (a) SR1, (c) SR2 and (e) SR3. (right) Cumulative zonal barotropic transports associated with MDT gradients, for (b) SR1, (d) SR2 and (f) SR3. SOSE (black), CNES-CLS09 (red), MN05 (blue), GGM02C (green), and EGM08 (magenta).

differences relative to SOSE (Table 3), we plot only initial misfit to EGM08 (Figure 1d) and note that the spatial structure is common for all products. The initial misfit shown in Figure 1d implies two types of discrepancies between SOSE and EGM08 (or the other MDT products). The large-scale north–south gradient in Figure 1d, with blue shading to the south of the ACC ($\bar{\eta}_{\mathrm{EGM08}} < \bar{\eta}_{\mathrm{SOSE}}$) and red to the north ($\bar{\eta}_{\mathrm{EGM08}} > \bar{\eta}_{\mathrm{SOSE}}$), implies a large-scale difference in the meridional MDT gradient. In addition Figure 1d also

Table 5. Normalized Cost When Initially Put in SOSE and After 10 Iterations of the Adjoint Method[a]

	Initial Cost	Cost After 10 Iterations	Percent Cost Decrease
$\langle(\bar{\eta}_{SOSE} - \bar{\eta}_{EGM08} + MDT_{T_c})^2\sigma_{MDT}^{-2}\rangle$	4.137	3.777	8.708
$\langle(\bar{\eta}_{SOSE} - \bar{\eta}_{EGM08})^2\sigma_{MDT}^{-2}\rangle$	1.909	1.520	20.370
$\langle(\bar{\eta}_{SOSE} - \bar{\eta}_{CNES-CLS09})^2\sigma_{MDT}^{-2}\rangle$	2.175	1.774	18.418
$\langle(\bar{\eta}_{SOSE} - \bar{\eta}_{GGM02C})^2\sigma_{MDT}^{-2}\rangle$	1.847	1.487	19.498
$\langle(\bar{\eta}_{SOSE} - \bar{\eta}_{MN05})^2\sigma_{MDT}^{-2}\rangle$	2.091	1.749	16.340
Total average MDT cost	2.357	1.986	15.733

[a]Normalized cost is the average misfit squared divided by uncertainty, σ_{MDT}, squared. The percent cost reduction is also given. The total MDT cost was about 1.3% of the overall total cost.

shows isolated patches with MDT differences as large as 0.5 m, particularly near Crozet and Kerguelen Islands in the south Indian Ocean and near the Campbell Plateau south of New Zealand, which are both associated with flow around specific bathymetric features.

[42] The 10 SOSE iterations carried out were insufficient to produce a fully converged solution, and costs descended steadily through all iterations. However, 10 iterations were sufficient to let us evaluate the general consistency of the state estimate solution with the MDT products. All four products showed significant cost reductions over the 10 iterations. This is an important result, as it shows that the MDT constraints provide information that is largely consistent with model physics and the majority of other observations. The cost reduction varied depending on the MDT product (Table 5). The greatest reduction was about 20% and was for the products derived solely from geoid observations: EGM08 and GGM02C. The products that combined ocean and geoid observations were less consistent with SOSE, as they had a cost about 10% higher, and the reduction was less significant: about 18% for CNES-CLS09 and 16% for MN05. The larger discrepancies between hybrid products and SOSE may stem from these products' extensive reliance on ocean surface drifter observations, which (as noted in section 1) tend to be biased in the Southern Ocean because of drogue losses [*Grodsky et al.*, 2011] and wind slip correction problems at high wind speeds [*Niiler et al.*, 2003; *Elipot and Gille*, 2009; *Grodsky et al.*, 2011]. This has the potential to result in an overestimate of surface ACC flow, and correspondingly an elevated meridional MDT gradient.

[43] However, products based solely on altimetry and gravity data also show an elevated MDT gradient, suggesting that the altimetry/gravity fields also have large-scale biases, perhaps associated with challenges in determining accurate MDT information near the seasonally varying ice of the Antarctic continent. Overestimation of ACC transport was also diagnosed in an inverse method in the SR3 section, as well as inconsistency between an older MDT product (CLS-SHOM98.2) and hydrography [*Losch and Schröter*, 2004]. *Andersen and Knudsen* [2009, Figure 11] compare DNSC08 MDT with OCCAM MDT and find a similar bias of the satellite product with respect to the model. It is unclear whether this bias is unique to the Southern Ocean. Earlier

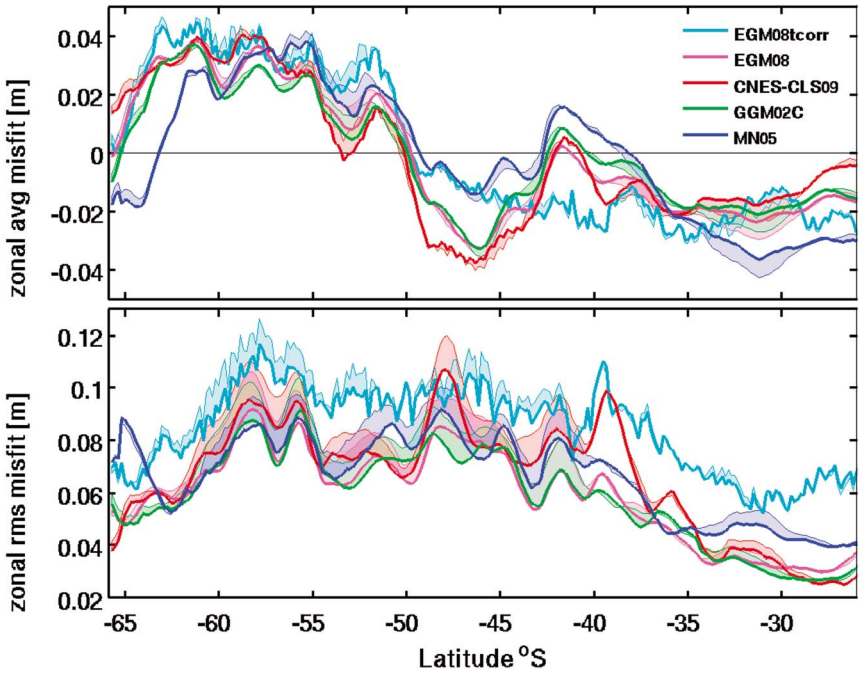

Figure 8. (top) Zonal mean and (bottom) root zonal mean square misfit, $\bar{\eta}_{SOSE} - \bar{\eta}_{MDT}$, for the EGM08 (magenta line), CNES-CLS09 (red line), GGM02C (green line), MN05 (blue line), and time-corrected EGM08 (black line) MDT products. The initial misfit (no optimization) is denoted with a thin line, while the thick line denotes the fit after 10 iterations of adjoint method optimization. The root zonal mean square fit was improved at almost all latitudes. The zonal mean misfit bias of an increased large-scale meridional gradient in the MDT products (i.e., compared to SOSE, the MDT products have lower $\bar{\eta}$ poleward of the ACC and greater $\bar{\eta}$ equatorward of the ACC) was not significantly reduced.

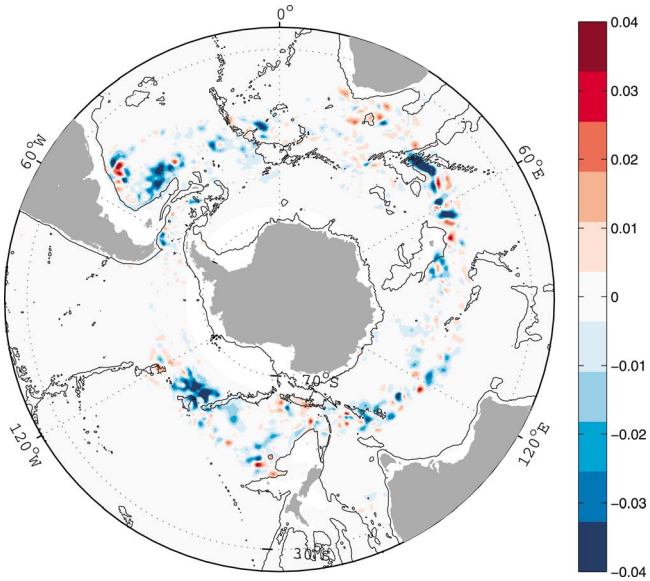

Figure 9. Change of squared misfit $((\bar{\eta}_{\mathrm{SOSE}_{\mathrm{initial}}} - \bar{\eta}_{\mathrm{EGM08}})2 - (\bar{\eta}_{\mathrm{SOSE}_{10}} - \bar{\eta}_{\mathrm{EGM08}})2)$ with respect to EGM08 after 10 iterations of the adjoint method in meters squared. Blue denotes region where the fit is improved (i.e., misfit was reduced). The 2800 m bathymetric contour is shown (black line). The change in fit is characterized by small-scale features occurring largely in regions where the influence of eddies and topography is strong.

analyses using a North Atlantic inverse model also showed overestimation of sea surface height gradients in MDT products [e.g., *Wunsch*, 1993; *Martel and Wunsch*, 1993], but we have not identified more recent analyses of this type.

[44] As discussed in section 2.2, one should account for discrepancies in the temporal sampling of the MDT constraints and the state estimate. However, this again proved nontrivial: our "time-corrected" version of the EGM08 MDT provided a poor constraint to SOSE, with double the cost of the other MDT constraints. As shown in Table 5, after 10 iterations, the cost reduced by just 8.7%. Further work is needed to determine how to properly account for the temporal sampling of the MDT products.

[45] Geographically, we find that in 10 iterations, the cost associated with the MDT products was reduced at all latitudes (Figure 8); however this was primarily achieved by reducing large magnitude local misfits, especially in the Argentine Basin (∼50°W), around Kerguelen (∼60°E), and in the Antarctic-Pacific Rise (∼130°W; see Figure 9). The large-scale zonal mean misfit (SOSE - MDT) was not substantially improved (Figure 8). The bias of ∼4 cm south of 55°S and ∼−3 cm north of 35°S implies the MDT products yield greater barotropic transport than SOSE. If the optimization had diminished this misfit, it would have likely resulted in significant changes to the SOSE solution due to interactions of the increased barotropic flow with the complex topography of the Southern Ocean. Of course, the barotropic transport can be compensated by baroclinic transport, and in this way leave bottom flows and topographic interactions unchanged. The baroclinic structure in SOSE, however, is well constrained by in situ measurements (e.g., Argo floats), and thus any baroclinic transport change would have to be consistent with the in situ observations. The fact that the optimization did not correct this misfit in the large-scale meridional gradient therefore suggests some inconsistencies between the meridional gradient in the MDT products and the dynamical (i.e., model physics) and hydrographic (i.e., in situ observation) constraints. However it is possible that if more iterations were carried out, the misfit reduction could increase and become more significant.

5. Summary and Discussion

[46] We have evaluated four widely used Southern Ocean MDT products along with the MDT diagnosed from SOSE. Our aim has been to evaluate the MDT products and their applicability to ACC transport estimates, to assess their uncertainties, and to use them as a constraint for a Southern Ocean assimilation.

[47] A priori uncertainties for the MDT products are not well characterized, but often assumed to be on the order of 10 cm in oceanographic applications [*Andersen and Knudsen*, 2009]. We found that RMS differences between the MDT products can reach 20 cm close to topographic features and where MDT gradients are large. These differences exceed the ∼10 cm magnitude assumed above, and should serve as a new lower bound on total uncertainty for MDT products.

[48] MDT products cannot easily be corrected to match a particular time period, and contrary to expectation, a time correction calculated from averaging and smoothing the gridded AVISO sea level anomaly product increases the RMS differences. MDT products (and particularly GGM02C, EGM08) filter out eddy scales in such a way that temporal variations in estimated MDT cannot be removed simply by subtracting out time-averaged altimetric sea surface heights for a particular time period. In addition, the identification of a representable time period for the MDT is problematic since the diverse data that have been used to calculate the MDT may refer to different, only partly overlapping, time periods themselves. *Andersen and Knudsen* [2009, Table 4] report time period corrections do slightly improve global RMS differences between two MDT products, but methods to determine the applied correction are not trivial.

[49] Compared with SOSE or historic hydrographic estimates, the MDT products generally exhibit larger meridional MDT gradients across the ACC, and imply a greater ACC transport. Hybrid products rely on surface drifter data that were designed to be drogued to follow ocean currents, but may experience uncorrected wind slip [*Niiler et al.*, 2003; *Elipot and Gille*, 2009; *Grodsky et al.*, 2011], which would result in an elevated transport and overestimated MDT gradients. However, the two altimetry/gravity-data-only products also exhibited a bias toward larger meridional MDT gradients as compared to SOSE and other observations. This could possibly be associated with challenges in using altimeters to determine the time-averaged sea surface height in the presence of sea ice. However, since the large-scale gradient is larger even away from the ice edge, it is unclear what other factors could lead to such a bias, and whether this bias is unique to the Southern Ocean. Clearly, further studies are needed to explore this issue with the large-scale gradient. Comparing different observational and modeled MDTs as a

function of filter scale, *Vossepoel* [2007] suggested that uncertainties at the larger spatial scales may not be much smaller than uncertainties at the smaller scales, and they conclude that improvement of mean sea surface estimates from satellite altimetry may be needed to improve MDT estimates at larger scales.

[50] The MDT products are generally inconsistent with the basic principle that the ocean circulation conserves mass. The calculations of transport from MDT products are sensitive to a number of factors including, among other things, the northern and southern limits used to estimate transport. We estimate the uncertainty in our transport calculation to be $\pm$24 Sv. However, this rather liberal uncertainty estimate is insufficient to account for the significant transport divergences inferred at the Southern Ocean choke points.

[51] The MDT products derived solely from altimeter and geoid observations (EGM08 and GGM02C) were found to be most consistent with SOSE. These constraints showed lower initial cost and almost 20% improvements after 10 iterations. Hybrid products might have been expected to perform well because of their extensive use of in situ ocean observations, but we found both the CNES-CLS09 and MN05 products had 10% higher initial costs than the altimetry/gravity-data-only products, and less reduction in misfit was achieved. The less successful convergence for the hybrid products may result from an uncalibrated wind slip correction in the surface drifter data that were influential in these products.

[52] While altimetry/gravity-data-only products do not suffer from the potential drifter errors that might bias the hybrid MDT fields, all products share a common trait that improvements in the RMS difference with SOSE was small scale and occurred in geographically isolated patches near topography where the influence of eddies is large. After 10 iterations, the large-scale north–south mismatch is not corrected. This suggests again a fundamental mismatch between SOSE and the MDT products at large scales and is not surprising in light of the choke point transport inconsistencies identified. SOSE has a strong transport conservation constraint, and therefore does not respond to the large-scale north–south MDT gradient in any of the MDT products.

[53] Our results imply that MDT estimates may be improved by adapting the calculation procedure to include a mass conservation constraint in the implied ocean circulations. Further work is needed to fully assess all of the contributors to uncertainty in the MDT products. This is in line with previous discussions of underestimated true geoid error and inconsistency of previous MDT products with hydrography in the framework of geostrophic dynamics [*Stammer et al.*, 2002; *Losch and Schröter*, 2004]. Future work must also determine the proper methodology to account for the temporal representation of the MDT products.

[54] **Acknowledgments.** We are grateful to Nikos Pavlis and to Bruce Cornuelle for helpful discussions. Deniz Varilsuha helped with analyses of CTD sections. MDT-CNES-CLS09 was produced by CLS Space Oceanography Division and distributed by Aviso, with support from CNES (http://www.aviso.oceanobs.com/). MN05 has been obtained from Nikolai Maximenko (IPRC) and Peter Niiler (SIO). We acknowledge http://grace.jpl.nasa.gov/data/dot/ for providing GGM02C. EGM08 was obtained via http://earth-info.nga.mil/GandG/wgs84/gravitymod/egm2008/.

References

Andersen, O. B., and P. Knudsen (2009), DNSC08 mean sea surface and mean dynamic topography models, *J. Geophys. Res.*, *114*, C11001, doi:10.1029/2008JC005179.

Bingham, R. J., and K. Haines (2006) Mean dynamic topography: intercomparisons and errors, *Philos. Trans. R. Soc.*, *364*, 903–916.

Bingham, R. J., K. Haines, and C. W. Hughes (2008), Calculating the ocean's mean dynamic topography from a mean surface and a geoid, *J. Atmos. Oceanic Technol.*, *25*, 1808–1822.

Chambers, D. P., J. Wahr, and R. S. Nerem (2004), Preliminary observations of global ocean mass variations with GRACE, *Geophys. Res. Lett.*, *31*, L13310, doi:10.1029/2004GL020461.

Chelton, D. B., J. C. Ries, B. J. Haines, L.-L. Fu, and P. S. Callahan (2001), Satellite altimetry, in *Satellite Altimetry and Earth Sciences*, edited by L.-L. Fu and A. Cazenave, pp. 1–131, Academic, San Diego, Calif.

Chereskin, T. K., K. A. Donohue, D. R. Watts, K. L. Tracey, Y. L. Firing, and A. L. Cutting (2009), Strong bottom currents and cyclogenesis in Drake Passage, *Geophys. Res. Lett.*, *36*, L23602, doi:10.1029/2009GL040940.

Cunningham, S. A., S. G. Alderson, B. A. King, and M. A. Brandon (2003), Transport and variability of the Antarctic Circumpolar Current in Drake Passage, *J. Geophys. Res.*, *108*(C5), 8084, doi:10.1029/2001JC001147.

Donohue, K. A., E. Firing, and L. Beal (2000), Comparison of three velocity sections of the Agulhas Current and Agulhas Undercurrent, *J. Geophys. Res.*, *105*, 28,585–28,593, doi:10.1029/1999JC000201.

Elipot, S., and S. T. Gille (2009), Estimates of wind energy input to the Ekman layer in the Southern Ocean from surface drifter data, *J. Geophys. Res.*, *114*, C06003, doi:10.1029/2008JC005170.

Foerste, C., et al. (2008), EIGEN-GL05C—A new global combined high-resolution GRACE-based gravity field model of the GFZ-GRGS cooperation, paper presented at General Assembly European Geosciences Union, Vienna, Austria 2008, Geophys. Res. Abstr., *10*, Abstract EGU2008-A-06944.

Ganachaud, A., and C. Wunsch (2000), Improved estimates of global ocean circulation, heat transport and mixing from hydrographic data, *Nature*, *408*, 453–457.

Georgi, S. T., and J. M. Toole (1982), The Antarctic Circumpolar Current and the oceanic heat and freshwater budgets, *J. Mar. Res.*, *40*, 183–197.

Gille, S. T. (2003), Float observations of the Southern Ocean: Part I: Estimating mean fields, bottom velocities, and topographic steering, *J. Phys. Oceanogr.*, *33*, 1167–1181.

Gouretski, V. V., and K. Jancke (1998), A new climatology for the World Ocean, *WOCE Rep. 162/98, Tech. Rep. 3*, WOCE Spec. Anal. Cent., Max-Planck Inst., Hamburg, Germany.

Griffies, S. M. (2004), *Fundamentals of Ocean Climate Models*, Princeton Univ. Press, Princeton, N. J.

Grodsky, S. A., R. Lumpkin, and J. A. Carton (2011), Spurious trends in global surface drifter currents, *Geophys. Res. Lett.*, *38*, L10606, doi:10.1029/2011GL047393.

Losch, M., and J. Schröter (2004), Estimating the circulation from hydrography and satellite altimetry in the Southern Ocean: limitations imposed by the current geoid models, *Deep Sea Res.*, *107*, 1131–1143.

Losch, M., B. M. Sloyan, J. Schröter, and N. Sneeuw (2002), Box inverse models, altimetry and the geoid: Problems with the omission error, *J. Geophys. Res.*, *107*(C7), 3078, doi:10.1029/2001JC000855.

Macdonald, A., and C. Wunsch (1996), An estimate of global ocean circulation and heat fluxes, *Nature*, *382*, 436–439.

Marshall, J., A. Adcroft, C. Hill, L. Perelman, and C. Heisey (1997), A finite-volume, incompressible Navier Stokes model for studies of the ocean on parallel computers, *J. Geophys. Res.*, *102*, 5753–5766, doi:10.1029/96JC02775.

Martel, F., and C. Wunsch (1993), Combined inversion of hydrography, current meter data and altimetric elevations for the North Atlantic circulation, *Manuscr. Geodaet.*, *18*, 219–266.

Maximenko, N. A., and P. P. Niiler (2005), Hybrid decade-mean global seal level with mesoscale resolution, in *Recent Advances in Marine Science and Technology*, edited by N. Saxena, pp. 55–59, PACON Int., Honolulu.

Maximenko, N., P. Niiler, L. Centurioni, M.-H. Rio, O. Melnichenko, D. Chambers, V. Zlotnicki, and B. Galperin (2009), Mean dynamic topography of the ocean derived from satellite and drifting buoy data using three different techniques, *J. Atmos. Oceanic Technol.*, *26*, 1910–1919.

Mazloff, M., P. Heimbach, and C. Wunsch (2010), An eddy-permitting Southern Ocean state estimate, *J. Phys. Oceanogr.*, *40*(5), 880–899, doi:10.1175/2009JPO4236.1.

Niiler, P. P., N. A. Maximenko, and J. C. McWilliams (2003), Dynamically balanced absolute sea level of the global ocean derived from near-surface velocity observations, *Geophys. Res. Lett.*, *30*(22), 2164, doi:10.1029/2003GL018628.

Pavlis, N. K., S. A. Holmes, S. C. Kenyon, and J. K. Factor (2008), An Earth gravitational model to degree 2160: EGM2008, *Geophys. Res. Abstr.*, *10*, Abstract EGU2008-A-01891.

Ponte, R. M., C. Wunsch, and D. Stammer (2007), Spatial mapping of time-variable errors in *Jason-1* and TOPEX/Poseidon sea surface height measurements, *J. Atmos. Oceanic Technol.*, *24*, 1078–1085.

Qiu, B. (1995), Variability and energetics of the Kuroshio Extension and its recirculation gyre from the first two years of TOPEX data, *J. Phys. Oceanogr.*, *25*, 1827–1842.

Reigber, C., et al. (2003), The CHAMP-only Earth Gravity Field Model EIGEN-2, *Adv. Space Res.*, *31*, 1883–1888.

Renault, A., C. Provost, N. Sennéchael, N. Barré, and A. Kartavtseff (2011), Two full-depth velocity sections in the Drake Passage in 2006—Transport estimates, *Deep Sea Res. Part II*, *58*, 2572–2591, doi:10.1016/j.dsr2.2011.01.004.

Rintoul, S. R., and S. Sokolov (2001), Baroclinic transport variability of the Antarctic Circumpolar Current south of Australia (WOCE repeat section SR3), *J. Geophys. Res.*, *106*, 2815–2832, doi:10.1029/2000JC900107.

Rio, M.-H., and F. Hernandez (2003), High-frequency response of wind-driven currents measured by drifting buoys and altimetry over the world ocean, *J. Geophys. Res.*, *108*(C8), 3283, doi:10.1029/2002JC001655.

Rio, M.-H., and F. Hernandez (2004), A mean dynamic topography computed over the world ocean from altimetry, in situ measurements, and a geoid model, *J. Geophys. Res.*, *109*, C12032, doi:10.1029/2003JC002226.

Rio, M.-H., P. Schaeffer, G. Moreaux, J.-M. Lemoine, and E. Bronner (2009), A new mean dynamic topography computed over the global ocean from GRACE data, altimetry and in-situ measurements, paper presented at OceanObs09 Symposium, Eur. Space Agency, Venice, Italy, 21–15 Sept.

Roach, A. T., K. Aagaard, C. H. Pease, S. A. Salo, T. Weingartner, V. Pavlov, and M. Kulakov (1995), Direct measurements of transport and water properties through the Bering Strait, *J. Geophys. Res.*, *100*, 18,443–18,457, doi:10.1029/95JC01673.

Sallée, J.-B., K. Speer, and R. Morrow (2008), Southern Ocean fronts and their variability to climate modes, *J. Clim.*, *21*, 3020–3039.

Sloyan, B. M., and S. R. Rintoul (2001), Circulation, renewal and modification of Antarctic mode and intermediate water, *J. Phys. Oceanogr.*, *32*, 1005–1030.

Sprintall, J., S. E. Wijffels, R. Molcard, and I. Jaya (2009), Direct estimates of the Indonesian Throughflow entering the Indian Ocean: 2004–2006, *J. Geophys. Res.*, *114*, C07001, doi:10.1029/2008JC005257.

Stammer, D., C. Wunsch, R. Giering, C. Eckert, P. Heimbach, J. Marotzke, A. Adcroft, C. N. Hill, and J. Marshall (2002), Global ocean circulation during 1992–1997, estimated from ocean observations and a general circulation model, *J. Geophys. Res.*, *107*(C9), 3118, doi:10.1029/2001JC000888.

Stammer, D., A. Koehl, and C. Wunsch (2007), Impact of accurate geoid fields on estimates of the ocean circulation, *J. Atmos. Ocean. Technol.*, *24*, 1464–1478.

Swenson, S., and J. Wahr (2006), Post-processing removal of correlated errors in GRACE data, *Geophys. Res. Lett.*, *33*, L08402, doi:10.1029/2005GL025285.

Tapley, B. D., and M. C. Kim (2000), Applications to geodesy, in *Satellite Altimetry and Earth Science*, *Int. Geophys. Ser.*, vol. 69, edited by A. Cazanave and L. L. Fu, pp. 371–406, Academic, New York.

Tapley, B. D., D. P. Chambers, S. Bettadpur, and J. C. Ries (2003), Large scale ocean circulation from the GRACE GGM01 Geoid, *Geophys. Res. Lett.*, *30*(22), 2163, doi:10.1029/2003GL018622.

Tapley, B. D., et al. (2005), GGM02—An improved Earth gravity field model from GRACE, *J. Geod.*, *79*, 467–478.

Tsaoussi, L. S., and C. J. Koblinsky (1994), An error covariance model for sea surface topography and velocity derived from TOPEX/POSEIDON altimetry, *J. Geophys. Res.*, *99*, 24,669–24,683, doi:10.1029/94JC01639.

Vossepoel, F. C. (2007), Uncertainties in the mean ocean dynamic topography before the launch of the Gravity Field and Steady-State Ocean Circulation Explorer (GOCE), *J. Geophys. Res.*, *112*, C05010, doi:10.1029/2006JC003891.

Whitworth, T. (1985), The net transport of the Antarctic Circumpolar Current through Drake Passage. *J. Phys. Oceanogr.*, *12*(9), 960–971.

Wunsch, C. (1993), Physics of the ocean circulation, in *Satellite Altimetry and Geodesy and Oceanography*, *Lect. Notes Earth Sci.*, vol. 50, edited by R. Rummel and R. Sanso, pp. 17–91, Springer, Berlin.

Wunsch, C. (1996), *The Ocean Circulation Inverse Problem*, 437 pp., Cambridge Univ. Press, Cambridge, U. K.

Wunsch, C., and P. Heimbach (2007), Practical global oceanic state estimation, *Physica D*, *230*, 197–208.

Zhang, Z., and Y. Lu (2005), Spectral analysis of mean dynamic topography from the GRACE GGM01 geoid, in *Gravity, Geoid and Space Missions*, *Int. Assoc. Geod. Symp.*, vol. 129, edited by L.-L. Fu and A. Cazenave, pp. 236–241, Springer, Berlin.

S. T. Gille, A. Griesel, and M. R. Mazloff, Scripps Institution of Oceanography, University of California, San Diego, 9500 Gilman Dr., La Jolla, CA 92093-0230, USA. (agriesel@ucsd.edu)